

Electronic Supplementary Information

β -Perfluoroalkyl-substituted pyrrole as an anion-responsive π -electronic system through a single NH moiety

Yohei Haketa, Ryota Takasago and Hiromitsu Maeda*

Department of Applied Chemistry, College of Life Sciences, Ritsumeikan University, Kusatsu 525–8577, Japan, E-mail: maedahir@ph.ritsumei.ac.jp

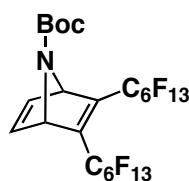
Table of contents

1. Synthetic procedures and spectroscopic data	S2
Supporting Figure 1–5 $^1\text{H}/^{13}\text{C}/^{19}\text{F}$ NMR spectra.	S4
2. X-ray crystallographic data	S12
Supporting Figure 6 Ortep drawing of single-crystal X-ray structure.	S12
Supporting Figure 7 Packing diagram of single-crystal X-ray structure.	S13
3. Optimization of pyrrole derivatives	S14
Supporting Figure 8 Optimized structures.	S14
Supporting Figure 9 Molecular orbitals.	S14
Supporting Figure 10 Electrostatic affinities of pyrroles for Cl^- .	S15
Cartesian coordination of optimized structures	S15
4. Anion-binding properties	S16
Supporting Figure 11–16 ^1H NMR spectral changes and curve fitting.	S16
5. Assembled behaviors and solid-state properties	S22
Supporting Figure 17 XRD pattern.	S22

1. Synthetic procedures and spectroscopic data

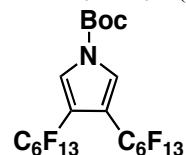
General procedures. Starting materials were purchased from Wako Pure Chemical Industries Ltd., Nacalai Tesque Inc., and Sigma-Aldrich Co. and used without further purification unless otherwise stated. NMR spectra used in the characterization of products were recorded on a JEOL ECA-600 600 MHz spectrometer. All NMR spectra were referenced to solvent. Matrix-assisted laser desorption ionization time-of-flight mass spectrometry (MALDI-TOF-MS) were recorded on a Shimadzu Axima-CFRplus using positive and negative mode. TLC analyses were carried out on aluminum sheets coated with silica gel 60 (Merck 5554). Column chromatography was performed on Wakogel C-300, and Merck silica gel 60 and 60H.

***N*-(*tert*-Butoxycarbonyl)-2,3-bis(tridecafluorohexyl)-7-azabicyclo[2.2.1]hepta-2,5-diene, **1**.** According to the literature procedure,^[S1] a 30 mL stainless steel autoclave charged with *N*-(*tert*-butoxycarbonyl)-1*H*-pyrrole^[S2] (1.0 g, 6.0 mmol) and tridecafluorotetradec-7-yne^[S3] (4.0 g, 6.0 mmol) was heated at 100 °C for 18 h. After cooling, the residue was then chromatographed over silica gel column (eluent: CH₂Cl₂/*n*-hexane = 1/3) to give **1** as a colorless oil (3.8 g, 4.0 mmol, 67%). *R_f* = 0.58 (CH₂Cl₂/*n*-hexane = 1/3). ¹H NMR (600 MHz, CDCl₃, 20 °C): δ (ppm) 7.13 (br, 2H, NCH), 5.53/5.45 (br, 2H, CH=CH), 1.42 (s, 9H, CH₃). ¹³C NMR (151 MHz, CDCl₃, 20 °C): δ (ppm) 153.28, 153.04, 151.56, 143.0, 82.46, 69.67, 27.92 (Multiple multiplet signals were observed at 120.41 ~ 106.66 ppm). ¹⁹F NMR (564 MHz, CDCl₃, 20 °C): δ (ppm) -82.08 ~ -82.09 (m, 6F), -107.94 ~ -108.65 (m, 2F), -113.31 ~ -114.20 (m, 2F), -120.64 ~ -122.26 (m, 4F), -123.19 (s, 4F), -124.09 (s, 4F), -127.44 (s, 4F). MALDI-TOF-MS: *m/z* (% intensity): 728.1 (100). Calcd for C₁₆H₂F₂₆N ([M - Boc]⁻): 727.99.

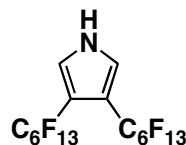


***N*-(*tert*-Butoxycarbonyl)-3,4-bis(tridecafluorohexyl)-pyrrole, **1c'**.** According to the literature procedure,^[S1] 2,4,6-trimethylbenzotriazole oxide (837.2 mg, 5.2 mmol) was added to a solution of **1** (3.8 g, 4.6 mmol) in Et₂O (17 mL). The mixture was stirred at r.t. for 24 h then evaporated. The residue was then chromatographed over silica gel column (eluent: CH₂Cl₂/*n*-hexane = 1/1) and recrystallized from CH₂Cl₂/*n*-hexane to give **1c'** as a colorless solid (3.3 g, 4.1 mmol, 89%; in the case of the presence of a small amount of *N*-Boc-pyrrole as an impurity with **1** as starting materials). *R_f* = 0.76 (CH₂Cl₂/*n*-hexane = 1/1). ¹H NMR (600 MHz, CDCl₃, 20 °C): δ (ppm) 7.61 (s, 2H, pyrrole-H), 1.65 (s, 9H, CH₃). ¹³C NMR (151 MHz, CDCl₃, 20 °C): δ (ppm)

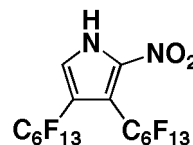
146.64, 124.12, 87.48, 27.87 (Multiple multiplet signals were observed at 120.25 ~ 106.73 ppm). ¹⁹F NMR (564 MHz, CDCl₃, 20 °C): δ (ppm) -82.10 (t, 6F), -104.65 (s, 4F), -121.76 (s, 4F), -122.99 (s, 4F), -124.13 (s, 4F), -127.44 (m, 4F). MALDI-TOF-MS: *m/z* (% intensity): 702.0 (100). Calcd for C₁₆H₂F₂₆N ([M]⁻): 701.98.



3,4-Bis(tridecafluorohexyl)-1*H*-pyrrole, **1c.** According to the literature procedure,^[S1] the compound **1c'** (594.4 mg, 0.74 mmol) was heated at 160 °C for 2 h. During the heating process, **1c** was sublimed as a white solid (508.7 mg, 0.72 mmol, 98%). *R_f* = 0.78 (CH₂Cl₂). ¹H NMR (600 MHz, CDCl₃, 20 °C): δ (ppm) 8.91 (br, 1H, NH), 7.20 (d, *J* = 3.0 Hz, 2H, CH). ¹³C NMR (151 MHz, CDCl₃, 20 °C): δ (ppm) 122.67 (Multiple multiplet signals were observed at 120.48 ~ 106.50 ppm). ¹⁹F NMR (564 MHz, CDCl₃, 20 °C): δ (ppm) -82.11 (t, 6F), -103.56 (s, 4F), -121.96 (s, 4F), -122.99 (s, 4F), -124.15 (s, 4F), -127.44 (s, 4F). MALDI-TOF-MS: *m/z* (% intensity): 702.0 (100). Calcd for C₁₆H₂F₂₆N ([M]⁻): 701.98.

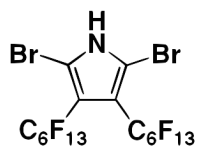


3,4-Bis(tridecafluorohexyl)-2-nitro-1*H*-pyrrole, **4a.** The solution of **1c** (19.0 mg, 27 μmol), H₂SO₄ (60 μL), and HNO₃ (60 μL) in CH₂Cl₂ (0.5 mL) was stirred for 7 h at r.t. The solution was washed with aq. Na₂CO₃ and dried over Na₂SO₄ and evaporated. After filtration with short silica pad, **4a** was obtained as a white solid (16.0 mg, 21.4 μmol, 78%). *R_f* = 0.29 (CH₂Cl₂). ¹H NMR (600 MHz, CDCl₃, 20 °C): δ (ppm) 10.86 (br, 1H, NH), 7.34 (s, 2H, CH). ¹⁹F NMR (564 MHz, CDCl₃, 20 °C): δ (ppm) -82.09 (t, 6F), -102.54 (s, 2F), -103.13 (s, 2F), -119.88 (s, 2F), -120.59 (s, 2F), -123.03 (s, 2F), -123.24 (s, 2F), -124.06 (s, 4F), -127.43 (s, 4F). MALDI-TOF-MS: *m/z* (% intensity): 746.6 (100). Calcd for C₁₆H₂F₂₆N₂O₂ ([M]⁻): 746.96.

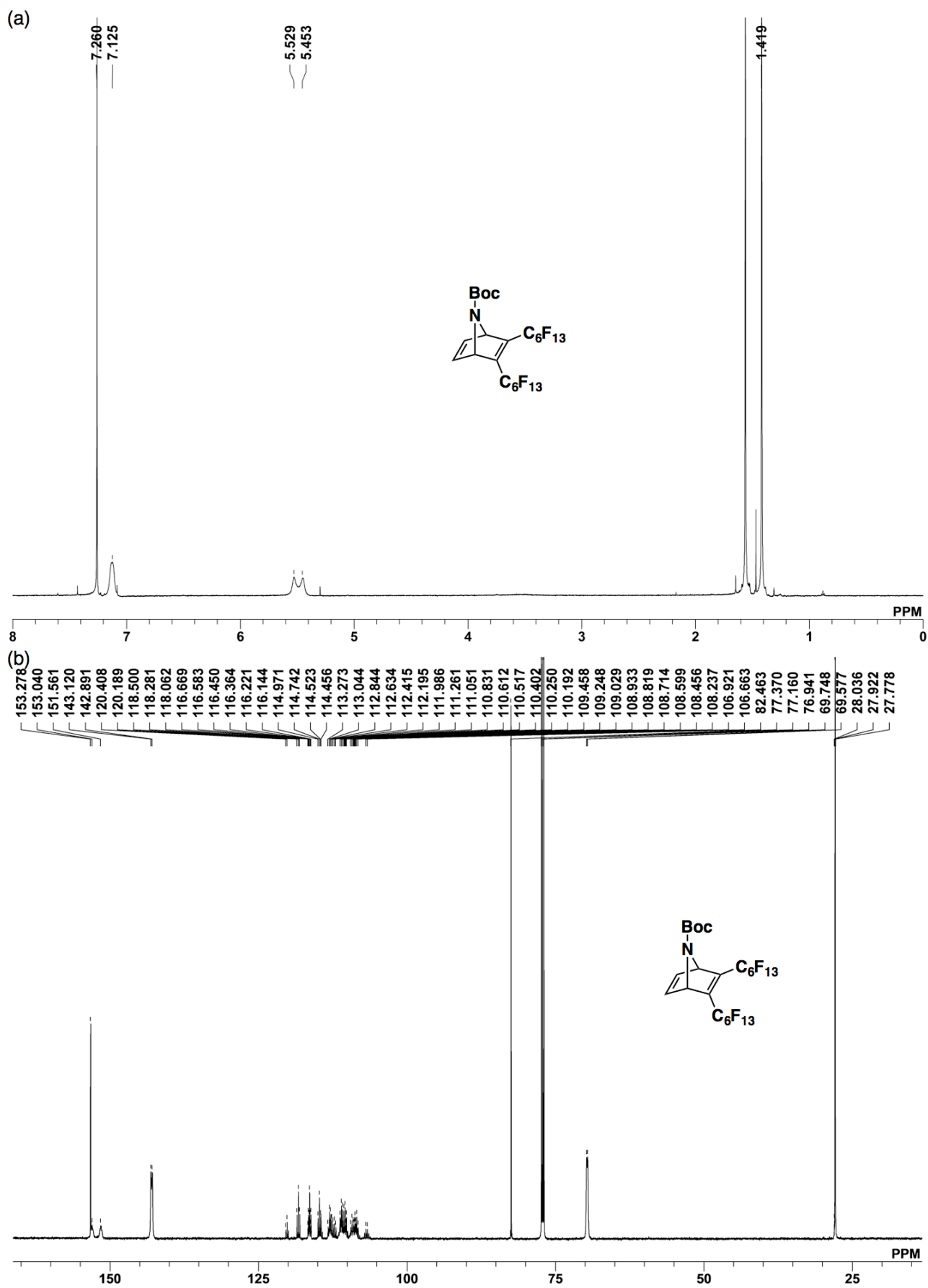


2,5-Dibromo-3,4-bis(tridecafluorohexyl)-1*H*-pyrrole, **4b.** The solution of **1c** (30 mg, 42 μmol) and Br₂ (80 μL) in CH₂Cl₂ (0.2 mL) was stirred for 48 h, then washed with aq. Na₂S₂O₃. After drying over Na₂SO₄ and evaporation, **4b** was obtained as a yellow solid (33.0 mg, 38.3 μmol, 90%). *R_f* = 0.49 (CH₂Cl₂/*n*-hexane =

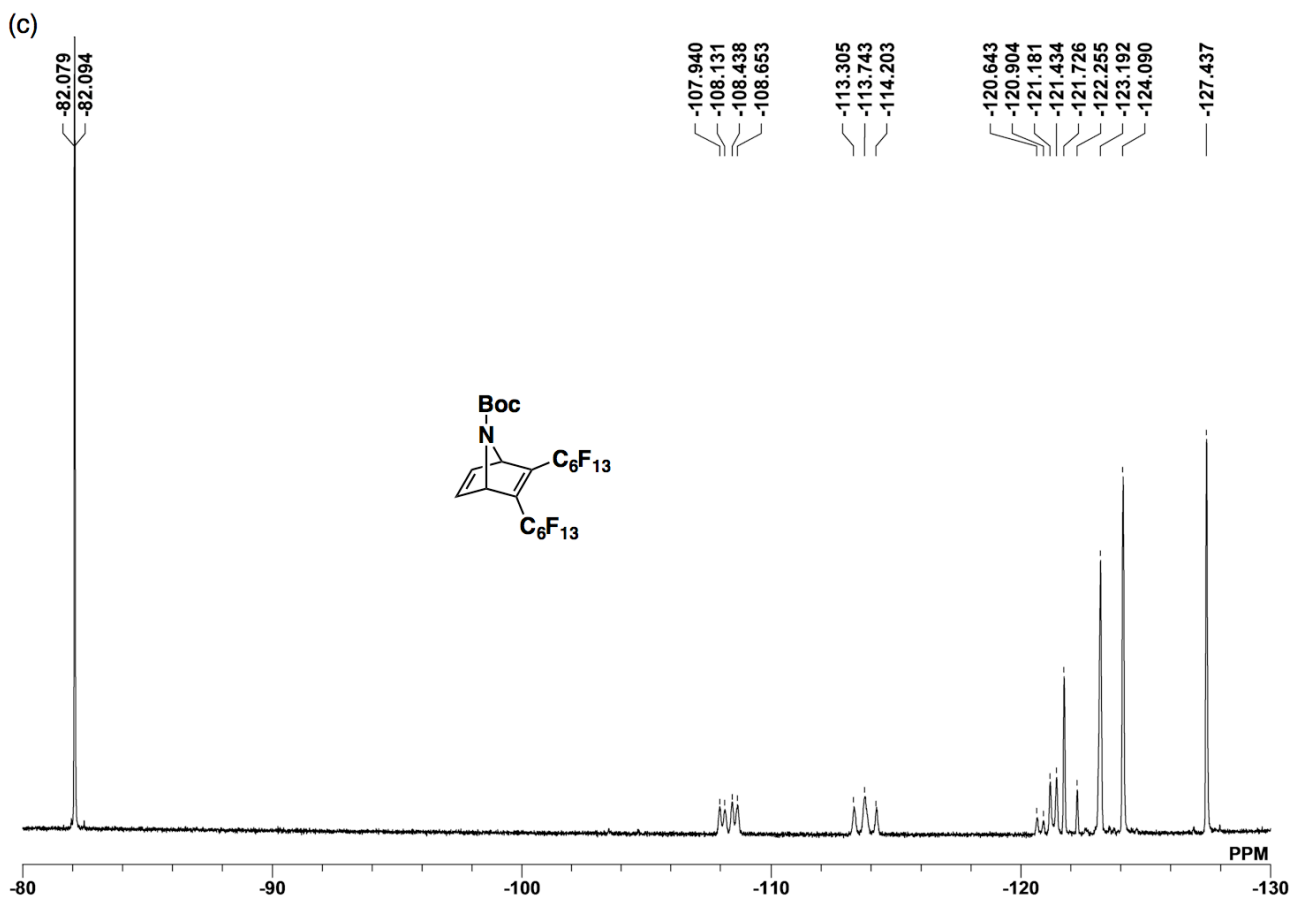
2/1). ^1H NMR (600 MHz, CDCl_3 , 20 °C): δ (ppm) 9.26 (br, 1H, NH). ^{19}F NMR (564 MHz, CDCl_3 , 20 °C): δ (ppm) -82.02 (t, 6F), -104.58 (s, 4F), -120.51 (s, 4F), -123.22 (s, 4F), -124.01 (s, 4F), -127.35 (s, 4F). MALDI-TOF-MS: m/z (% intensity): 857.8 (100). Calcd for $\text{C}_{16}\text{Br}_2\text{F}_{26}\text{N}$ ($[\text{M}]^+$): 857.80.



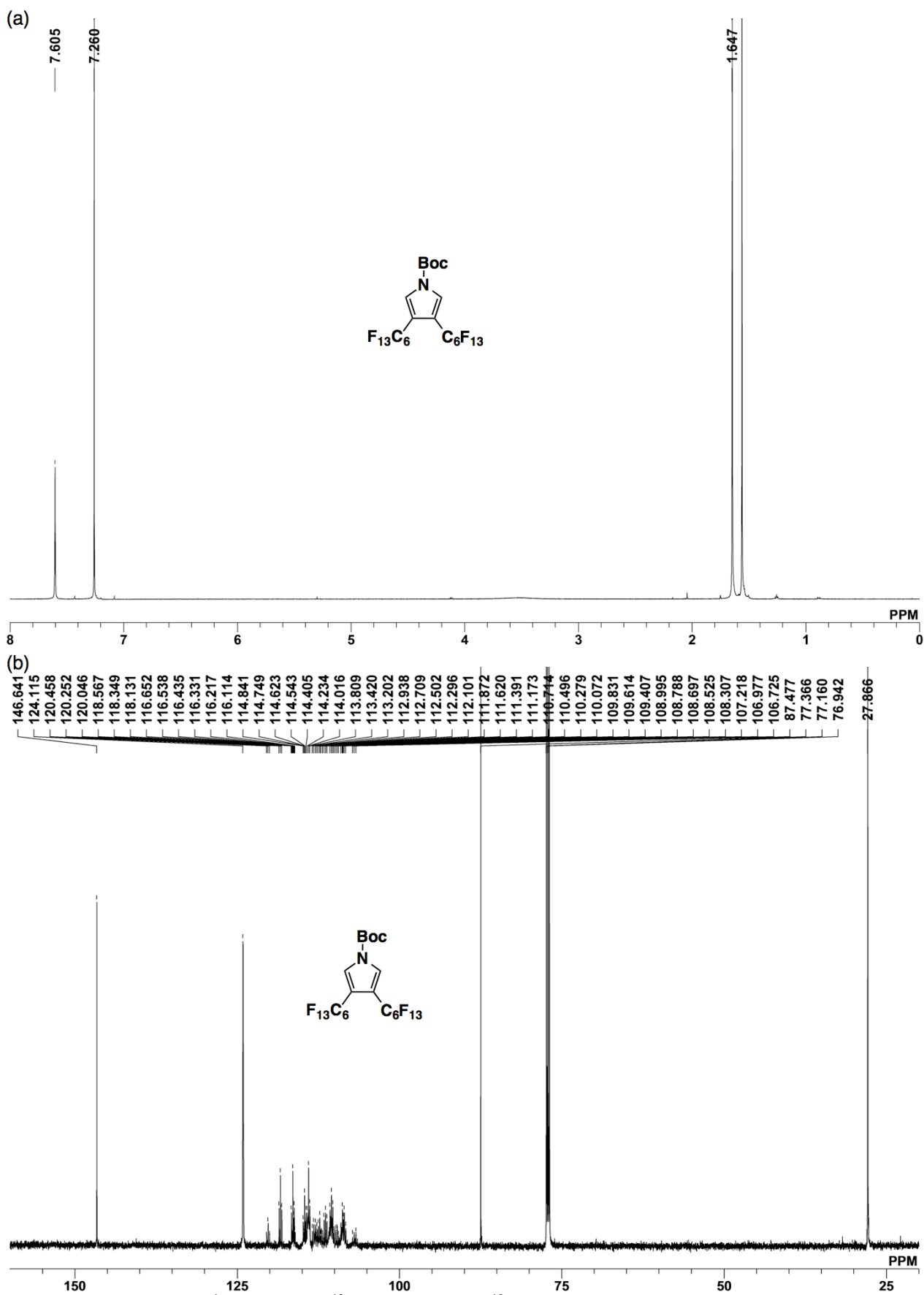
- [S1] J. Leroy, D. Cantacuzene and C. Wakselman, *Synthesis*, 1982, 313–315.
[S2] H. Salman, Y. Abraham, S. Tal, S. Melzman, M. Kapon, N. Tessler, S. Speiser and Y. Eichen, *Eur. J. Org. Chem.*, 2005, 2207–2212.
[S3] J. Lim and T. M. Swager, *Angew. Chem. Int. Ed.*, 2010, **49**, 7486–7488.



Supporting Figure 1 (a) ^1H NMR, (b) ^{13}C NMR, and (c) ^{19}F NMR spectra of **s1** in CDCl_3 at 20°C . In (c), complicated split signals at $-116.71 \sim -118.32$ ppm are derived from the stereoisomers of perfluorohexyl unit located in the *trans*-position, providing one perfluorohexyl unit proximal to *N*-Boc unit.

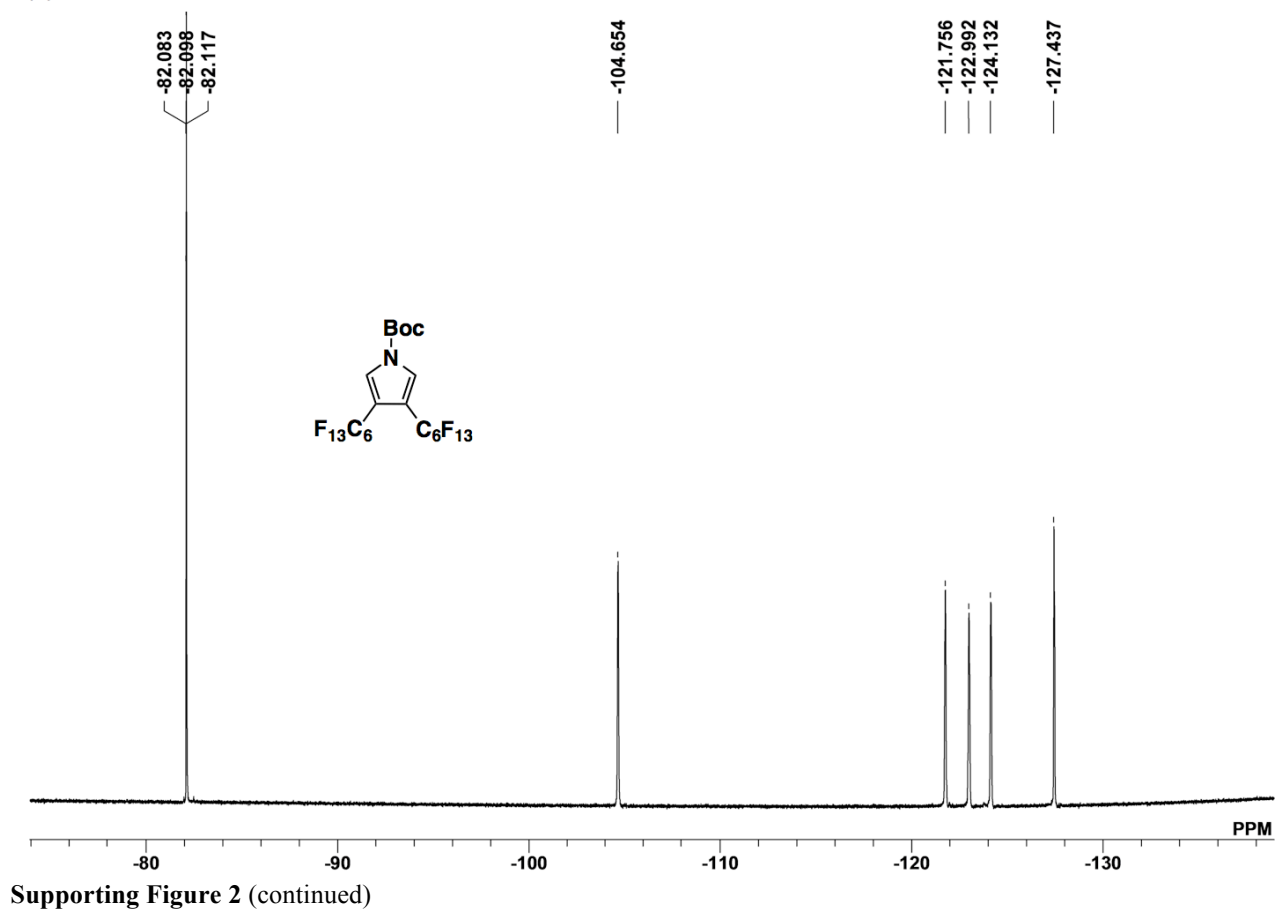


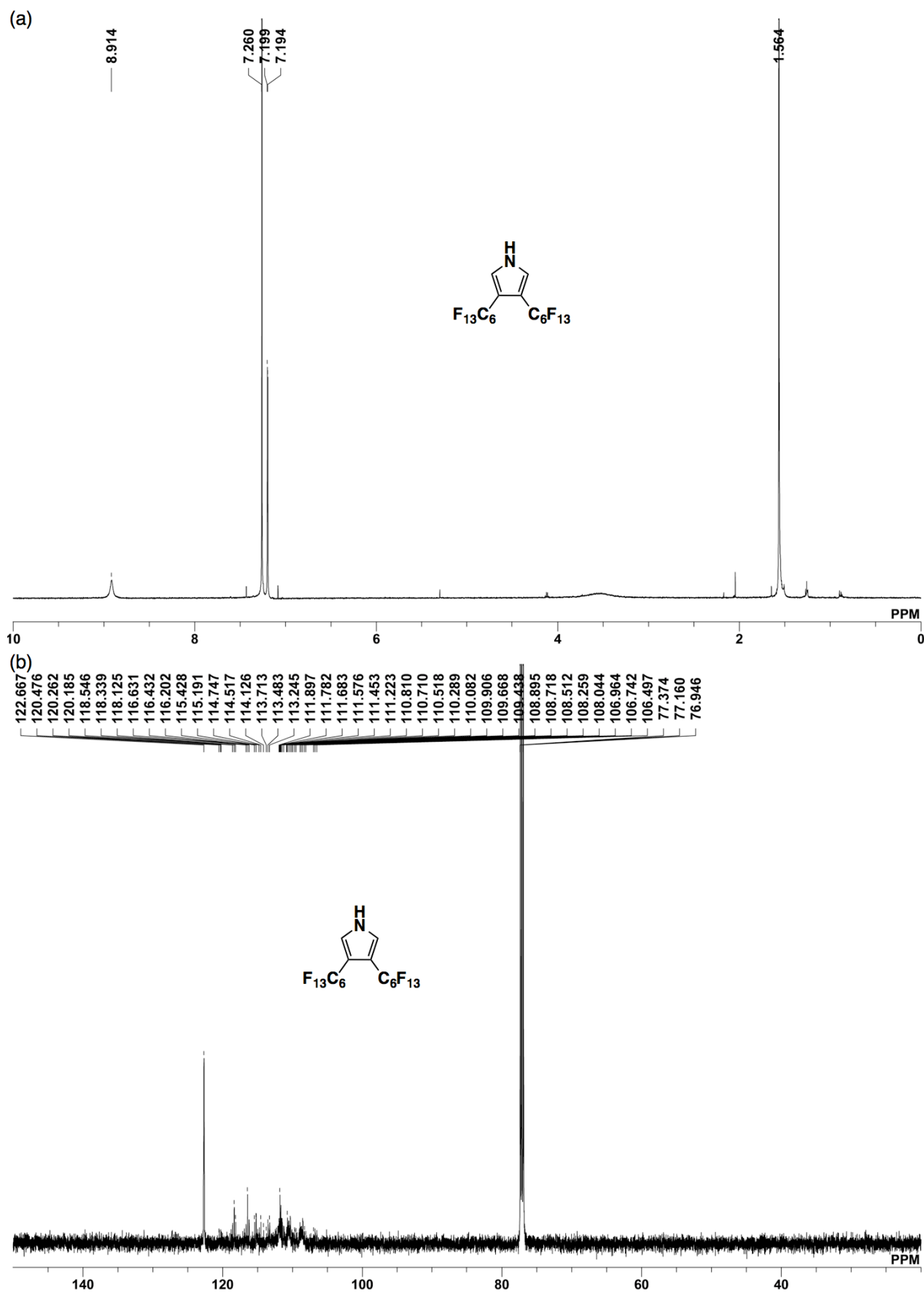
Supporting Figure 1 (continued)



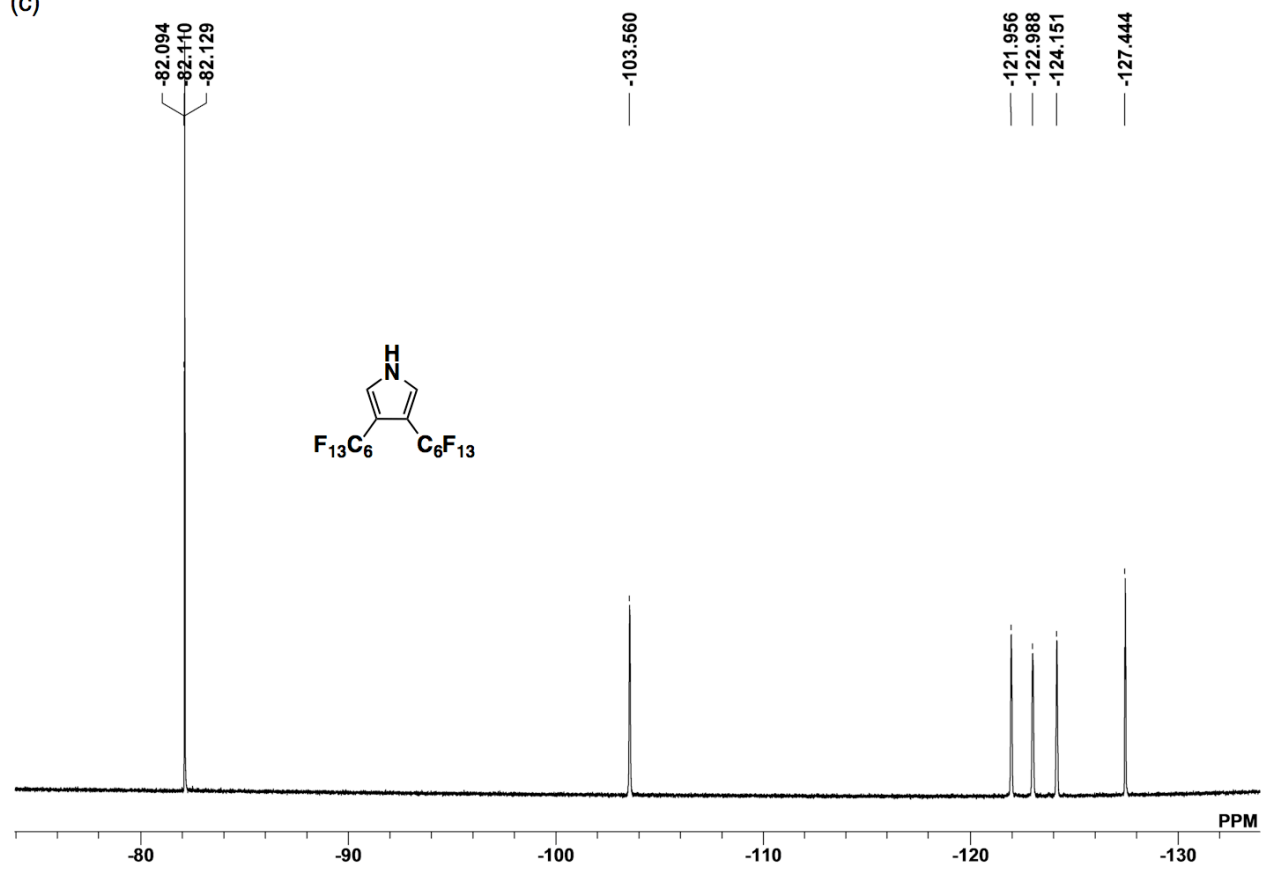
Supporting Figure 2 (a) ^1H NMR, (b) ^{13}C NMR, and (c) ^{19}F NMR spectra of **1c'** in CDCl_3 at 20°C . In (b), complicated split signals at $120.25 \sim 106.73$ ppm derived from the perfluorohexyl units. Pyrrole β -carbon was not clearly observed due to the coupling with a neighboring CF_2 moiety.

(c)





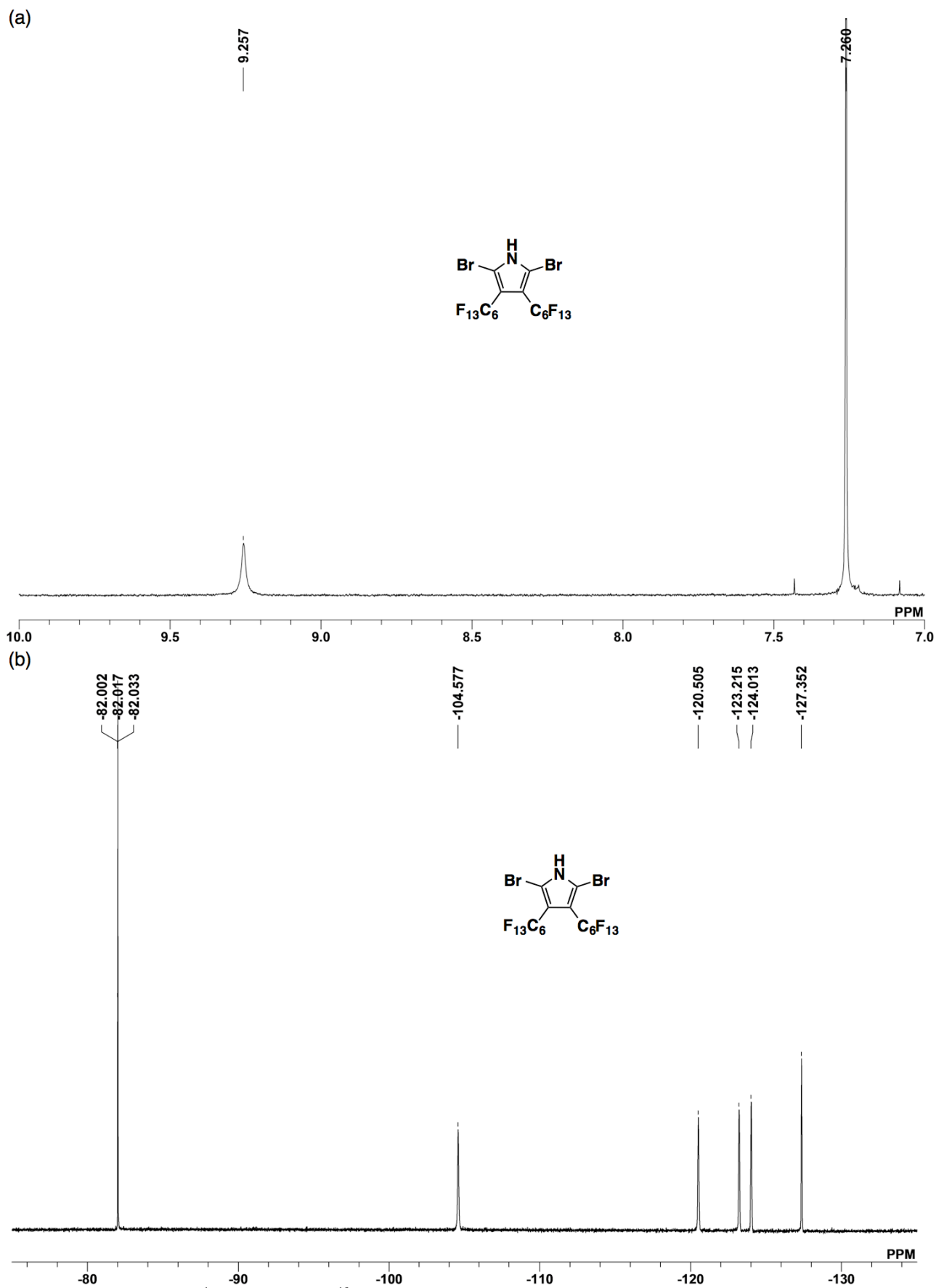
(c)



Supporting Figure 3 (continued)



Supporting Figure 4 (a) ^1H NMR and (b) ^{19}F NMR spectra of **4a** in CDCl_3 at 20 $^\circ\text{C}$.

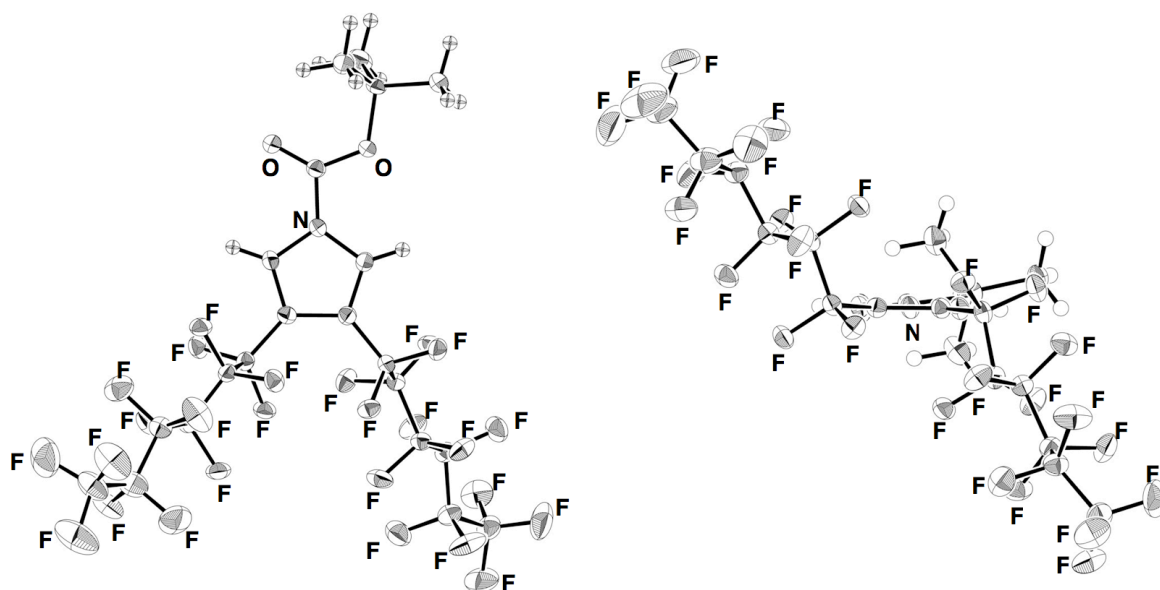


2. X-ray crystallographic data

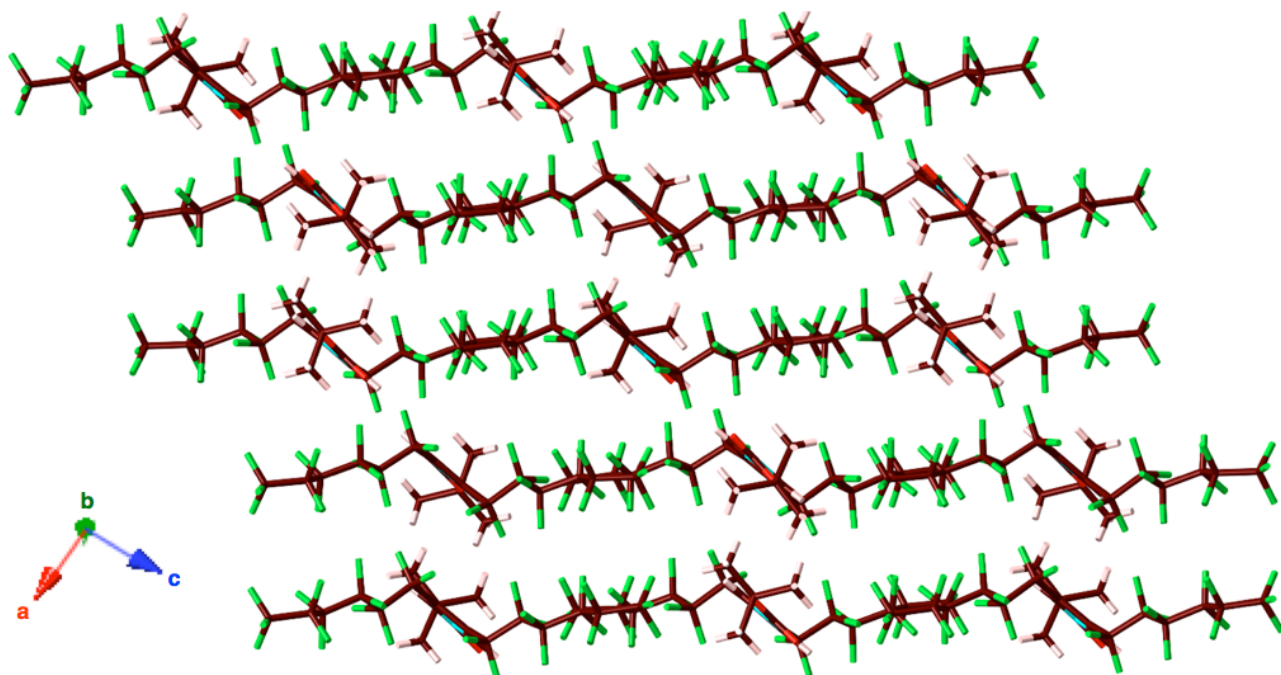
Method for single-crystal X-ray analysis. Crystallographic data for **1c'** is summarized in Supporting Table 1. A single crystal of **1c'** was obtained by vapor diffusion of *n*-decane into a CHCl₃ solution. The data crystal was a colorless prism of approximate dimensions 0.49 mm × 0.25 mm × 0.05 mm. Data were collected at 93 K on a Rigaku XtaLAB P200 diffractometer with graphite monochromated Cu-K α radiation ($\lambda = 1.54187 \text{ \AA}$), and structure was solved by direct method. The non-hydrogen atoms were refined anisotropically. The calculations were performed using the Crystal Structure crystallographic software package of Molecular Structure Corporation.^[S4] A CIF file (CCDC-1476278) can be obtained free of charge from the Cambridge Crystallographic Data Centre via www.ccdc.cam.ac.uk/data_request/cif.

Supporting Table 1 Crystallographic details for the compound **1c'**.

	1c'
formula	C ₄₂ H ₂₂ F ₅₂ N ₂ O ₂
fw	1600.62
crystal size, mm	0.49 × 0.25 × 0.05
crystal system	triclinic
space group	<i>P</i> -1 (no. 2)
<i>a</i> , Å	12.370(3)
<i>b</i> , Å	12.834(4)
<i>c</i> , Å	18.490(5)
α , °	98.783(18)
β , °	91.487(6)
γ , °	104.872(7)
<i>V</i> , Å ³	2797.3(13)
ρ_{calcd} , gcm ⁻³	1.907
<i>Z</i>	2
<i>T</i> , K	93(2)
μ , mm ⁻¹ (Cu-K α)	2.234
no. of reflns	35192
no. of unique reflns	9502
variables	901
λ , Å (Cu-K α)	1.54187
<i>R</i> ₁ (<i>I</i> > 2 σ (<i>I</i>))	0.0505
<i>wR</i> ₂ (<i>I</i> > 2 σ (<i>I</i>))	0.1455
<i>GOF</i>	1.059



Supporting Figure 6 Ortep drawing of single-crystal X-ray structure (top and side view) of **1c'**. Thermal ellipsoids are scaled to the 50% probability level.

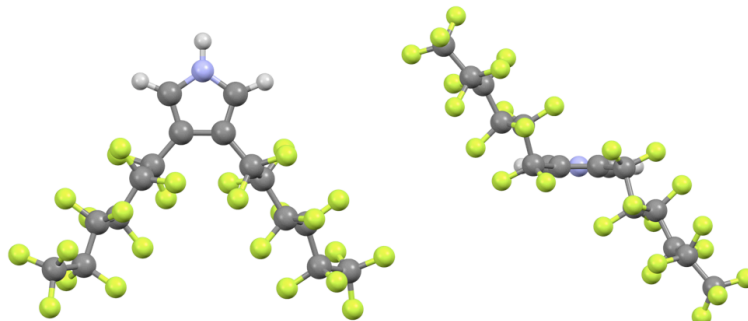


Supporting Figure 7 Packing diagram of **1c'**. Atom color code: brown, pink, green, blue, and red refer to carbon, hydrogen, fluorine, nitrogen, and oxygen, respectively.

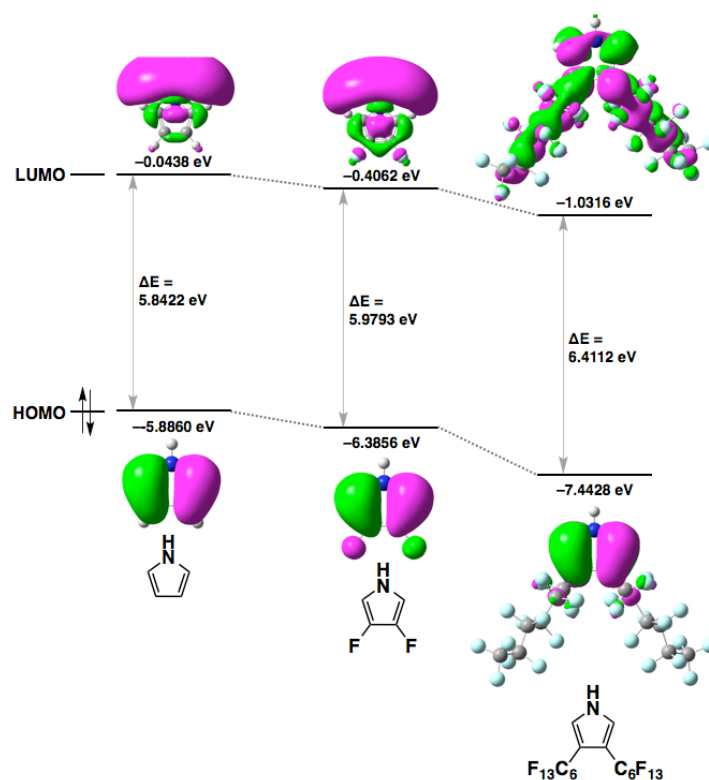
[S4] *CrystalStructure (Ver. 3.8), Single Crystal Structure Analysis Software*, Rigaku/MSC and Rigaku Corporation, 2006.

3. Optimization of pyrrole derivatives

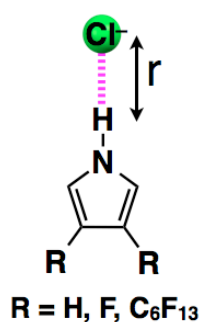
DFT calculations. DFT calculations for pyrrole derivatives were carried out by using *Gaussian 09* program.^[S5] The structures were optimized at B3LYP/6-31G(d,p) for anion-free pyrroles and B3LYP/6-31+G(d,p) for pyrrole–anion complexes. The total electronic energies in both cases along with molecular orbitals (MO) and electrostatic potentials (ESP) were calculated at B3LYP/6-31+G(d,p).



Supporting Figure 8 Optimized structure (top and side view) of **1c** at B3LYP/6-31G(d,p) level.



Supporting Figure 9 Molecular orbitals (HOMO and LUMO) of **1a–c** at B3LYP/6-31+G(d,p)//B3LYP/6-31G(d,p) level, suggesting that the substitution of electron-withdrawing moieties at pyrrole β -positions decrease HOMO and LUMO energy levels, wherein decreasing HOMO level is larger than that of LUMO level, resulting in a larger HOMO/LUMO gap.



$$U_E = \frac{1}{4 \cdot \pi \cdot \epsilon_0} \sum_{i=1}^n \frac{q_i \cdot q_{Cl}}{r_i}$$

U_E ... electrostatic energy

q_i ... point charge of constituting atoms of pyrrole

q_{Cl} ... point charge of Cl⁻

r_i ... the distance between Cl⁻ and constituting atoms of pyrrole

ϵ_0 ... vacuum permittivity

Supporting Figure 10 The interactions between pyrrole derivatives and Cl⁻ were evaluated by means of electrostatic energy (U_E) between Cl⁻ and the constituting atoms of pyrroles (the sum of the U_E of Cl⁻ and each atom). Point charges (q_i and q_{Cl}) of the constituting atoms in pyrrole–Cl⁻ complexes (the total charge of –1) were estimated based on the natural charges, which were evaluated by natural population analysis using DFT calculations at the level of B3LYP/6-31+G(d,p)//B3LYP/6-31G(d,p). The distances between Cl⁻ and the constituting atoms of pyrroles (r_i) were calculated using the coordinates of pyrrole–Cl⁻ obtained from the DFT calculations. From abovementioned values, U_E for **1a** (β-H), **1b** (β-F), and **1c** (β-C₆F₁₃) were estimated as –14.3, –23.7, and –30.7 kcal/mol, respectively, clearly indicating the larger affinities for Cl⁻ by the pyrrole derivatives with more electron-withdrawing substituents.

Cartesian Coordination of **1c** (DFT)

-3262.0472826 hartree

C,0.8720178956,4.0303831796,0.7050479701

C,0.5528080525,2.7121856868,0.456810627

C,-0.5527974984,2.7121918815,-0.4568088947

C,-0.8719904191,4.0303928693,-0.7050493821

N,0.0000179582,4.8134300036,-0.0000005846

H,0.0000241388,5.8214196227,-0.0000013358

H,1.6494347934,4.4497012813,1.3234596996

H,-1.6494002716,4.4497195668,-1.3234641236

C,-1.3423536438,1.5761260246,-1.0201090998

C,1.3423570517,1.5761115661,1.0201046126

C,-2.5432357445,1.1518919921,-0.1181833938

C,2.5432169804,1.1518568304,0.1181596312

F,-0.5713806564,0.4722898666,-1.2281378463

F,-3.4565418602,2.1602661716,-0.1556280402

F,-2.1102699477,1.0088668519,1.1555759698

F,-1.8778066734,1.953051031,-2.2220554775

F,1.8778361449,1.9530341175,2.2220401414

F,0.5713737036,0.4722861903,1.2281514623

F,3.4565137648,2.1602418319,0.15553921

F,2.1102137767,1.0087786745,-1.1555813157

C,3.2474785944,-0.1746788554,0.5329671767

C,4.6585986019,-0.3589362886,-0.1065512913

C,5.1875354853,-1.8210977974,-0.0413009146

C,6.7086677648,-1.9623776105,-0.320364315

C,-3.2474721517,-0.1746675311,-0.5329599799

C,-4.6586029331,-0.3589201243,0.1065372895

C,-5.187521367,-1.8210906398,0.0413307523

C,-6.7086611211,-1.96237906,0.3203492562

F,-3.3981304556,-0.2056620114,-1.8773412437

F,-2.4627970559,-1.2090896993,-0.1494242673

F,-4.6136991782,0.0089417763,1.4085929823

F,-5.53178883,0.4436698131,-0.548965982

F,-4.9510043678,-2.3300261623,-1.1911879865

F,-4.5323041323,-2.5600677456,0.9630911886

F,-7.0050559628,-3.260206987,0.4625096511

F,-7.4243856601,-1.4671602659,-0.6948673731

F,-7.0402251968,-1.3170354489,1.4474021214

F,3.3981631881,-0.2056228725,1.8773467971

F,2.4628100516,-1.2091251277,0.1494824091

F,5.5317882328,0.4436881,0.5489049713

F,4.613665273,0.0088762286,-1.4086197481

F,4.5322955223,-2.560120015,-0.9630085638

F,4.9510658831,-2.3299845812,-1.1912470369

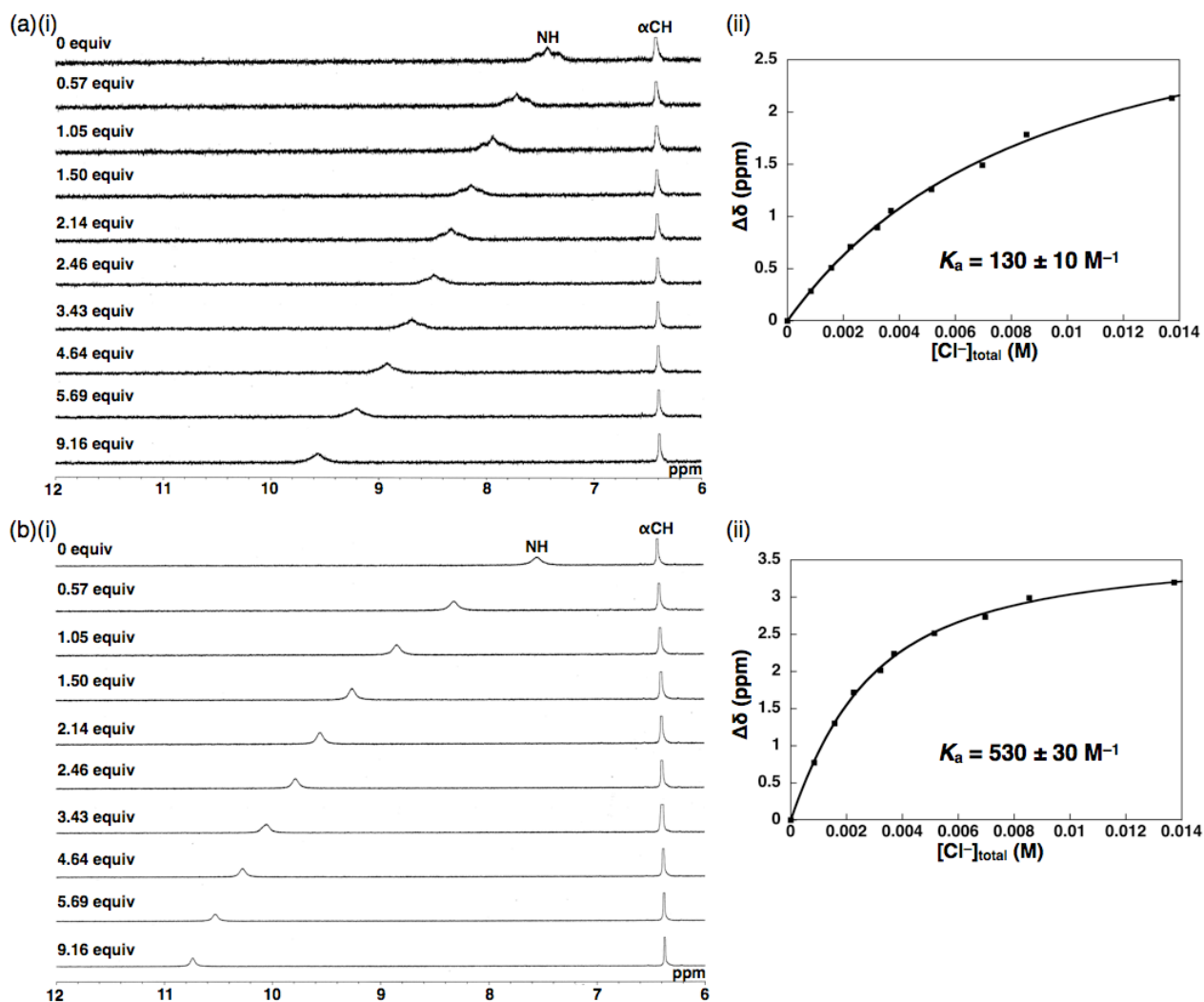
F,7.0401832609,-1.3170867234,-1.4474616205

F,7.4244188123,-1.4670942034,0.6948022737

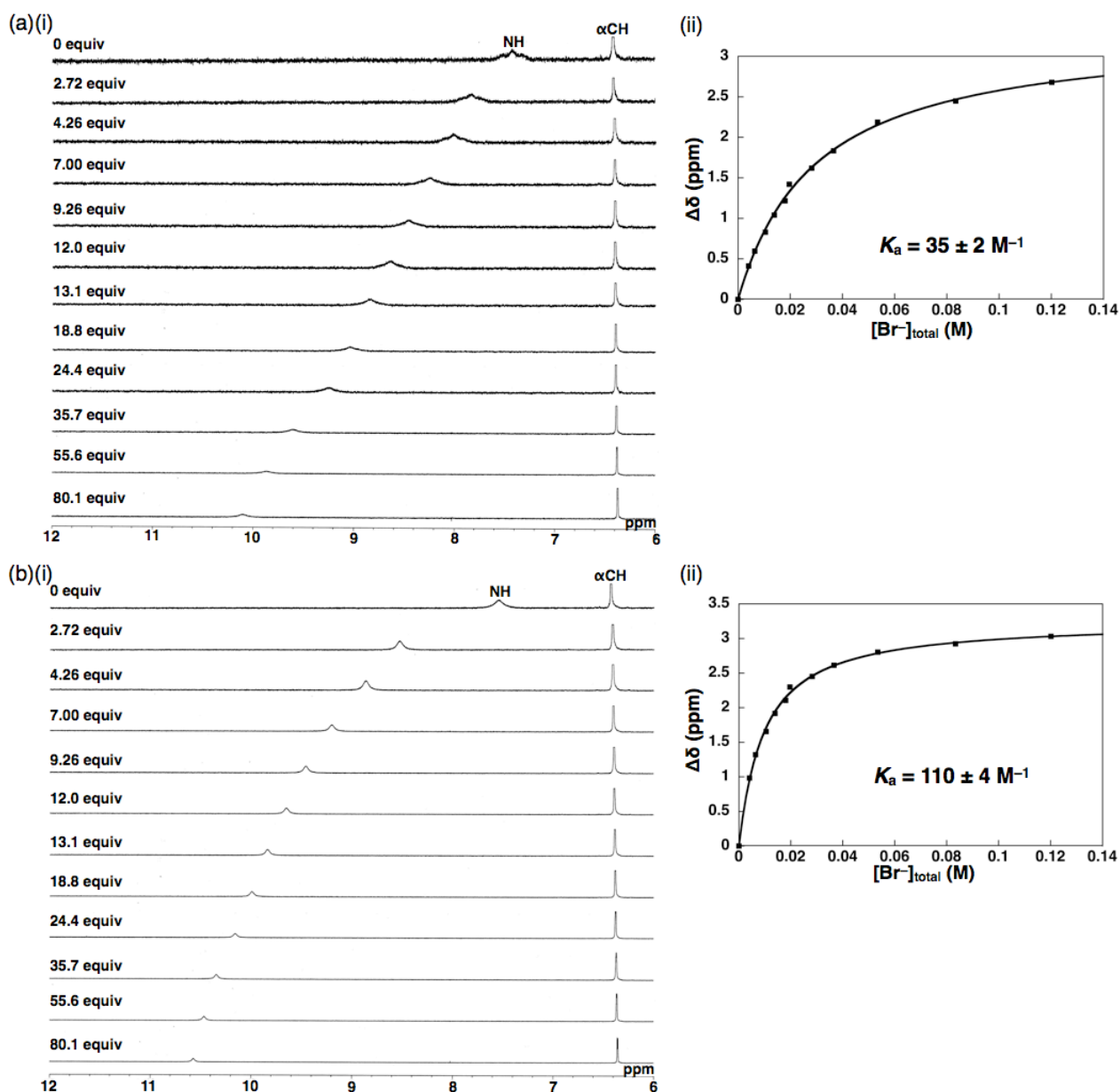
F,7.0050782065,-3.2602081372,-0.4624671905

[S5 (complete ref. 13)] *Gaussian 09* (Revision D.01), M. J. Frisch, G. W. Trucks, H. B. Schlegel, G. E. Scuseria, M. A. Robb, J. R. Cheeseman, G. Scalmani, V. Barone, B. Mennucci, G. A. Petersson, H. Nakatsuji, M. Caricato, X. Li, H. P. Hratchian, A. F. Izmaylov, J. Bloino, G. Zheng, J. L. Sonnenberg, M. Hada, M. Ehara, K. Toyota, R. Fukuda, J. Hasegawa, M. Ishida, T. Nakajima, Y. Honda, O. Kitao, H. Nakai, T. Vreven, J. A. Montgomery, Jr., J. E. Peralta, F. Ogliaro, M. Bearpark, J. J. Heyd, E. Brothers, K. N. Kudin, V. N. Staroverov, T. Keith, R. Kobayashi, J. Normand, K. Raghavachari, A. Rendell, J. C. Burant, S. S. Iyengar, J. Tomasi, M. Cossi, N. Rega, M. J. Millam, M. Klene, J. E. Knox, J. B. Cross, V. Bakken, C. Adamo, J. Jaramillo, R. Gomperts, R. E. Stratmann, O. Yazyev, A. J. Austin, R. Cammi, C. Pomelli, J. W. Ochterski, R. L. Martin, K. Morokuma, V. G. Zakrzewski, G. A. Voth, P. Salvador, J. J. Dannenberg, S. Dapprich, A. D. Daniels, Ö. Farkas, J. B. Foresman, J. V. Ortiz, J. Cioslowski and D. J. Fox, Gaussian, Inc., Wallingford CT, 2013.

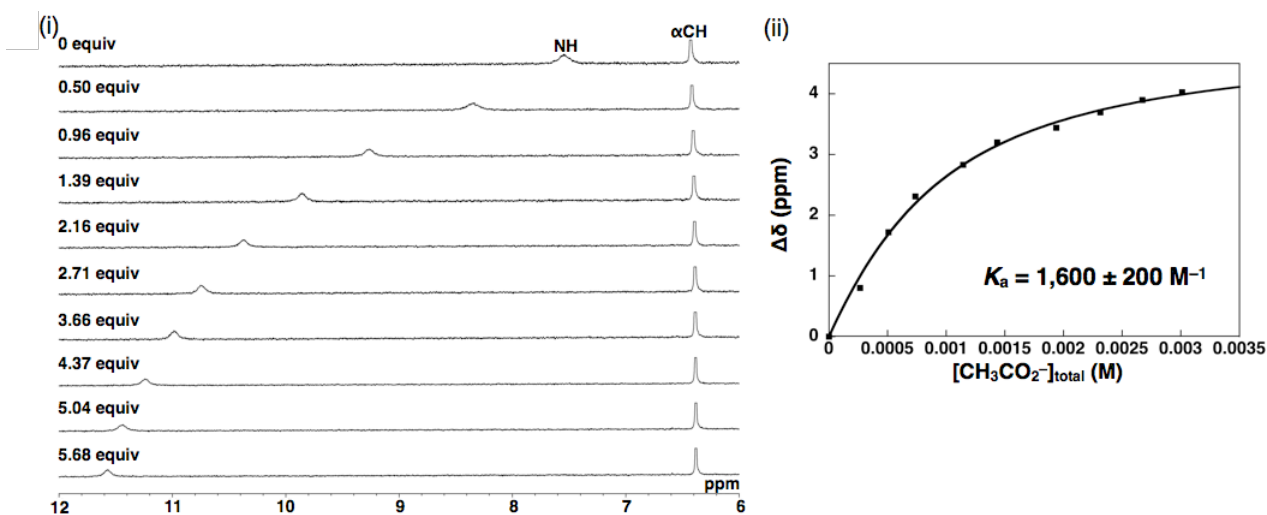
4. Anion-binding properties



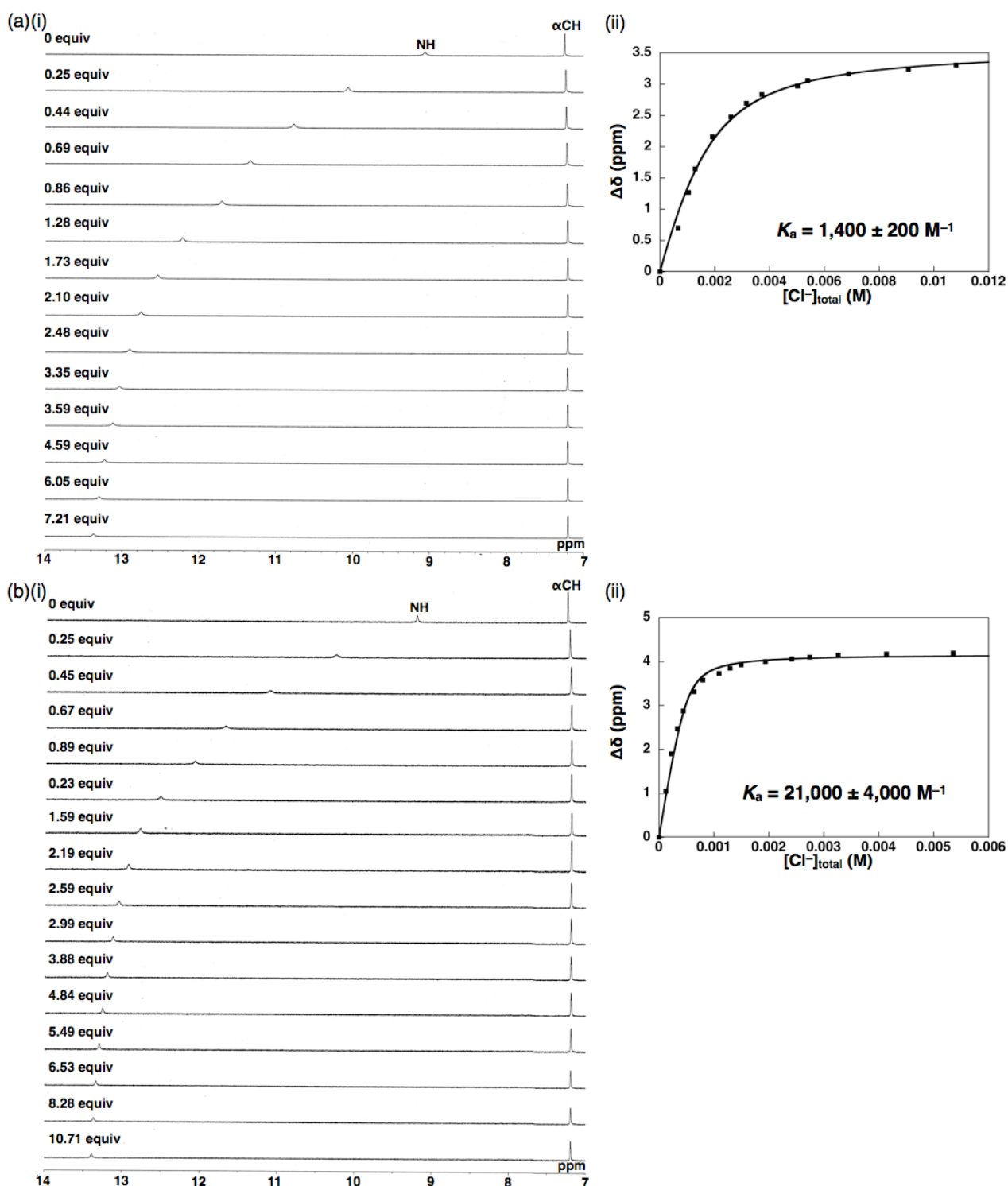
Supporting Figure 11 (i) ¹H NMR spectral changes and (ii) corresponding [1+1] anion-binding curve fitting of **1b** ($1.5 \times 10^{-3} \text{ M}$) in CD_2Cl_2 at (a) 20 °C and (b) -50 °C upon the addition of Cl⁻ added as a tetrabutylammonium (TBA) salt. As shown in (ii), shifts of pyrrole-NH signals upon the addition of anion well fit to nonlinear least-square [1+1]-binding curves, suggesting the formation of a [1+1]-type anion complex.



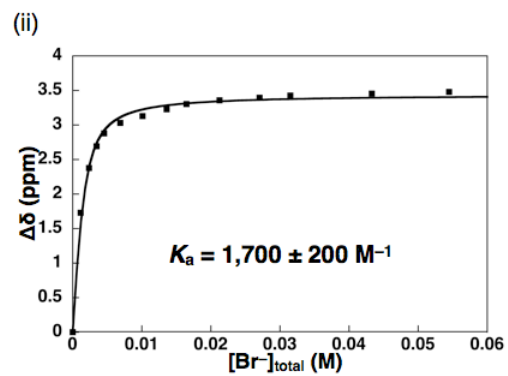
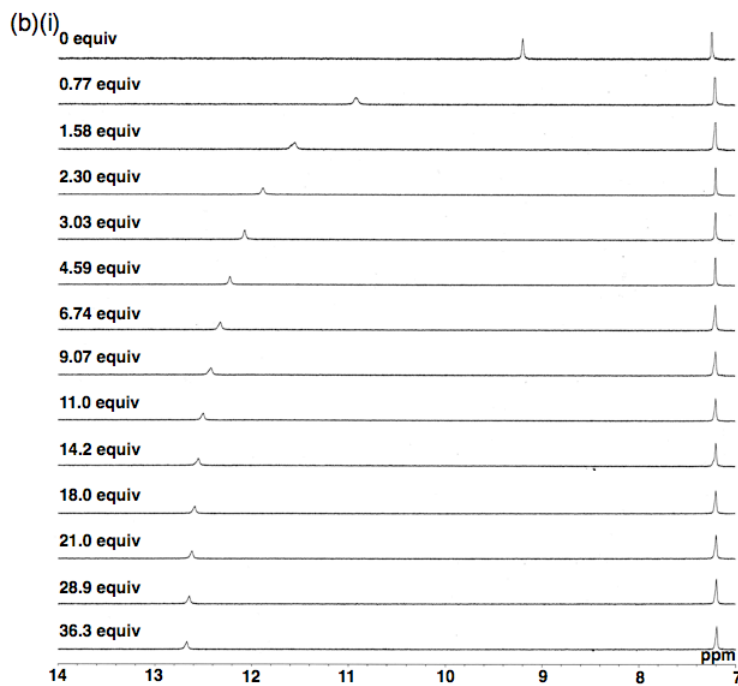
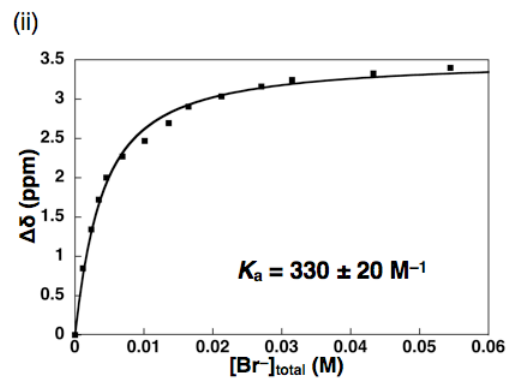
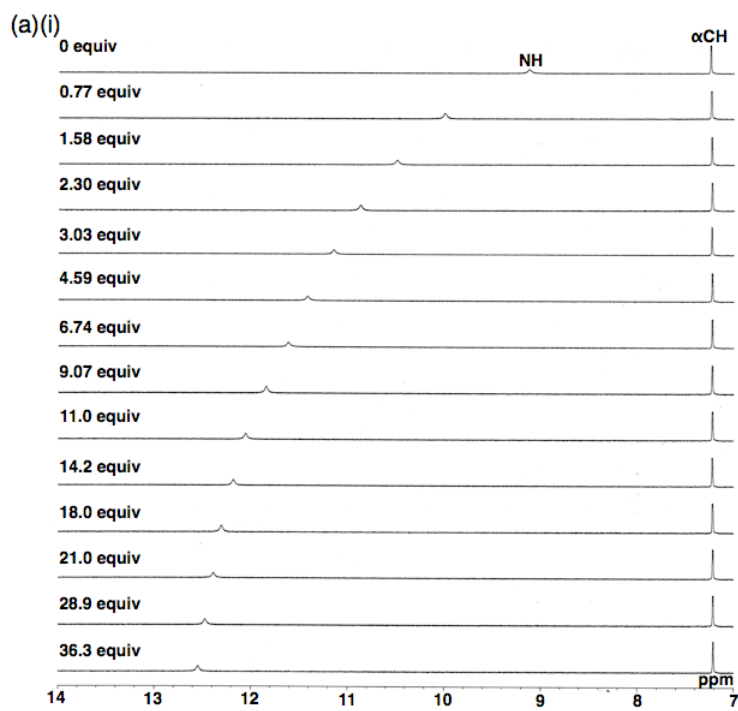
Supporting Figure 12 (i) ^1H NMR spectral changes and (ii) corresponding [1+1] anion-binding curve fitting of **1b** ($1.5 \times 10^{-3} \text{ M}$) in CD_2Cl_2 at (a) 20°C and (b) -50°C upon the addition of Br^- added as a TBA salt.



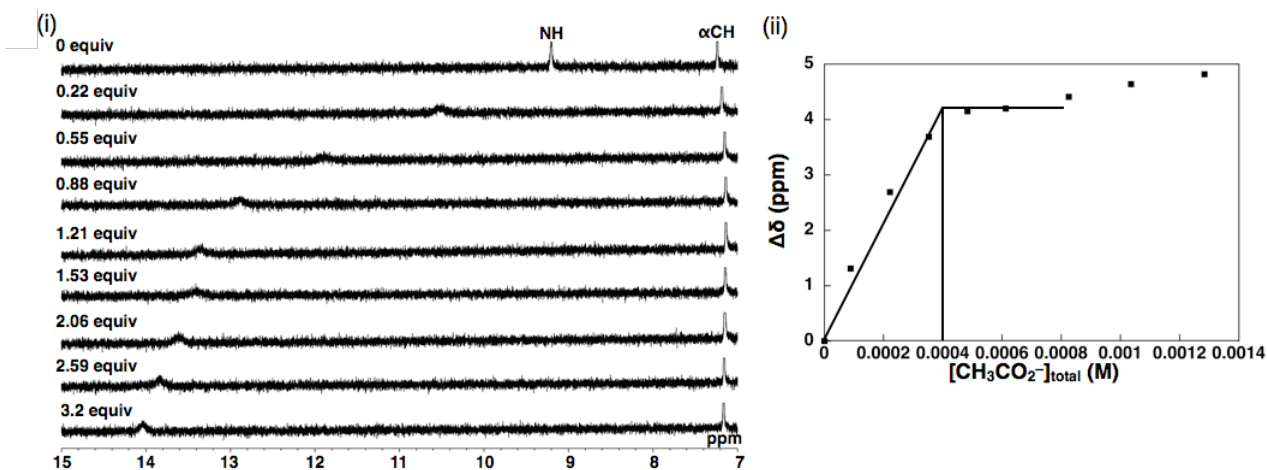
Supporting Figure 13 (i) ¹H NMR spectral changes and (ii) corresponding [1+1] anion-binding curve fitting of **1b** (5 × 10⁻⁴ M) in CD₂Cl₂ at -50 °C upon the addition of CH₃CO₂⁻ added as a TBA salt. Spectral changes at 20 °C are omitted due to the broad pyrrole-NH signals derived from a fast exchange between **1b** and **1b**·Cl⁻.



Supporting Figure 14 (i) ^1H NMR spectral changes and (ii) corresponding [1+1] anion-binding curve fitting of **1c** in CD_2Cl_2 at (a) $20\text{ }^\circ\text{C}$ ($1.5 \times 10^{-3}\text{ M}$) and (b) $-50\text{ }^\circ\text{C}$ ($5 \times 10^{-4}\text{ M}$) upon the addition of Cl^- added as a TBA salt.



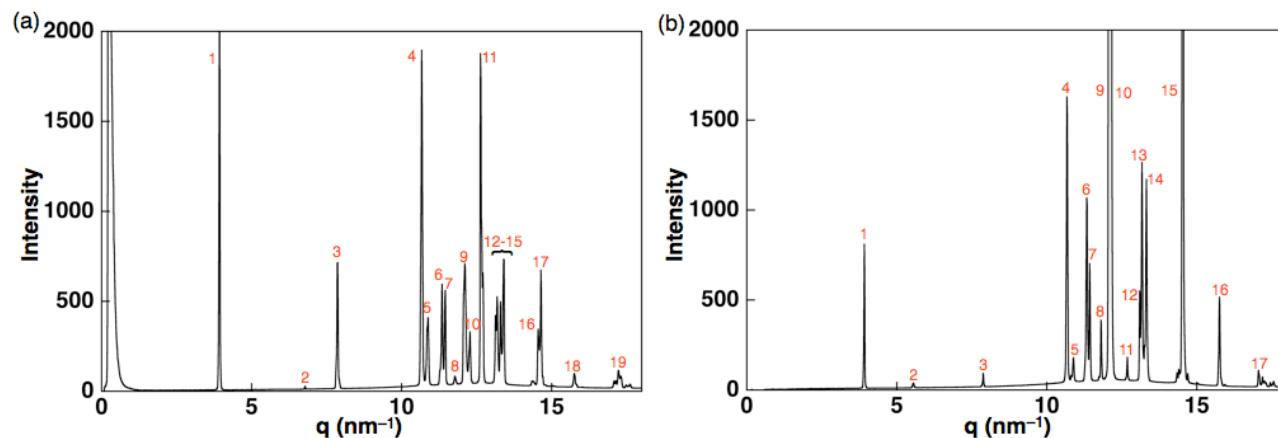
Supporting Figure 15 (i) ^1H NMR spectral changes and (ii) corresponding [1+1] anion-binding curve fitting of **1c** (1.5×10^{-3} M) in CD_2Cl_2 at (a) 20 °C and (b) -50 °C upon the addition of Br^- added as a TBA salt.



Supporting Figure 16 (i) ^1H NMR spectral changes and (ii) corresponding [1 + 1] anion-binding curve fitting of **1c** (4×10^{-4} M) in CD_2Cl_2 at -50 °C upon the addition of CH_3CO_2^- added as a TBA salt, suggesting that the K_a value for CH_3CO_2^- was too high in this conditions to exactly estimate. Therefore, the rough estimation by assuming that the [1+1] complex was formed in 90% upon the addition of 1 equiv of CH_3CO_2^- provided $K_a > 10^5 \text{ M}^{-1}$. Furthermore, the addition of more than 2 equiv of CH_3CO_2^- resulted in the continuous NH peak shift as another process, probably the deprotonation at NH. Spectral changes at 20 °C are omitted due to the broad pyrrole-NH signals derived from a fast exchange between **1c** and **1c**·Cl⁻.

5. Assembled behaviors and solid-state properties

Synchrotron X-ray diffraction analysis (XRD). High-resolution XRD analysis was carried out using a synchrotron radiation X-ray beam with a wavelength of 1.00 Å on BL40B2 at SPring-8 (Hyogo, Japan). A large Debye-Scherrer camera with a camera length of 540.108 mm using a quartz capillary, was used with an imaging plate as a detector, where the diffraction patterns were obtained with a 0.01° step in 2θ. The exposure time to the X-ray beam was 10 sec.



Supporting Figure 17 XRD patterns of **1c** at 25 °C as the solid state (a) before and (b) after melting at the isotropic liquid (Iso). Labeled numbers at each peaks are listed in Supporting Table 2. Solid-state **1c** shows complicated XRD patterns, suggesting the highly ordered crystalline state.

Supporting Table 2 XRD peaks of **1c** at 25 °C (a) before and (b) after melting.

	peak no.	q (nm ⁻¹)	d-spacing (nm)	ratio	hkl
(a) before melting	1	3.932	1.598	1.000	
	2	6.783	0.926	0.580	
	3	7.870	0.798	0.500	
	4	10.676	0.588	0.368	
	5	10.879	0.577	0.361	
	6	11.355	0.553	0.346	
	7	11.456	0.548	0.343	
	8	11.773	0.533	0.334	
	9	12.113	0.518	0.325	
	10	12.282	0.511	0.320	
	11	12.633	0.497	0.311	
	12	13.131	0.478	0.299	
	13	13.188	0.476	0.298	
	14	13.301	0.472	0.296	
	15	13.403	0.469	0.293	
	16	14.557	0.431	0.270	
	17	14.647	0.429	0.268	
	18	15.756	0.399	0.250	
	19	17.227	0.365	0.228	
(b) after melting	1	3.921	1.602	1.000	
	2	5.550	1.132	0.706	
	3	7.881	0.797	0.497	
	4	10.676	0.588	0.367	
	5	10.891	0.577	0.360	
	6	11.332	0.554	0.346	
	7	11.434	0.549	0.343	
	8	11.807	0.532	0.332	
	9	12.079	0.520	0.325	
	10	12.147	0.517	0.323	
	11	12.690	0.495	0.309	
	12	13.097	0.479	0.299	

Supporting Table 2 (continued)

13	13.176	0.477	0.298
14	13.323	0.471	0.294
15	14.534	0.432	0.270
16	15.756	0.399	0.249
17	17.057	0.368	0.230
